Bioorganic Chemistry 84 (2019) 295–301

Contents lists available at ScienceDirect

Bioorganic Chemistry

journal homepage: www.elsevier.com/locate/bioorg

# Artemisianins A-D, new stereoisomers of seco-guaianolide involved heterodimeric [4 + 2] adducts from *Artemisia argyi* induce apoptosis via enhancement of endoplasmic reticulum stress

Gui-Min Xue, Dong-Rong Zhu, Chao Han, Xiao-Bing Wang, Jian-Guang Luo*, Ling-Yi Kong*

*Jiangsu Key Laboratory of Bioactive Natural Product Research and State Key Laboratory of Natural Medicines, School of Traditional Chinese Pharmacy, China Pharmaceutical University, 24 Tong Jia Xiang, Nanjing 210009, People's Republic of China*

ARTICLE INFO

*Keywords:*
*Artemisia argyi*
Seco-guaianolide sesquiterpenoid dimer
Stereoisomer
Structure elucidation
Endoplasmic reticulum stress

ABSTRACT

Artemisianins A-D (**1**–**4**), four stereoisomers of sesquiterpenoid dimers, forming via [4 + 2] cycloaddition from a 1, 10-seco-guaianolide dienophile and a guaianolide diene, along with two biosynthetically related precurors **5** and **6**, were isolated from the famous traditional Chinese medicine *Artemisia argyi*. The structures of **1**–**4**, including their absolute configurations, were elucidated by extensive spectroscopic data and ECD/TDDFT calculation analysis. Compounds **1**–**4** exhibited cytotoxicity with $IC_{50}$ values ranging from 7.2 to 23.3 μM. The accumulation of $Ca^{2+}$ in cytoplasm and enlarged endoplasmic reticulum (ER) indicated that **1** mediated HT-29 cancer cell apoptosis through improvement of ER-stress, which was further proved by unfolded protein response (UPR) pathway on basis of the upregulation of IRE1α, p-PERK, ATF6, and CHOP.

## 1. Introduction

Dimeric sesquiterpenoids (DSs) are a group of secondary metabolites, naturally having $C_{30}$ cores, which are always originated biosynthetically from two sesquiterpenoid units [1–3]. Compared with sesquiterpenoid monomers, DSs have a relatively limited distribution [1]. Investigation has revealed that the most of DSs occur in higher plants, especially dicotyledons, and only a few of them are reported from higher fungi and ferns [1,2]. In recent years, DSs have attracted considerable attention owing to their great structural variety and widely ranging of biological activities, including anti-tumor [4,5], and anti-inflammation [6,7].

The plants from *Artemisia* species have been reported as a rich source of novel dimeric guaianolides [8–10]. *Artemisia argyi*, belonging to this genus, is a famous traditional medicine commonly known as silvery wormwood or Chinese mugwort (Aiye). Traditionally, the herb is considered to increase the blood supply to the pelvic region and stimulate menstruation, help treat infertility, dysmenorrhea, asthma and coughs. Their leaves are always used as an antiseptic, expectorant, febrifuge and styptic. Previous phytochemical investigation on *A. argyi* has led to discovery of several guaianolide dimers biosynthesized from two complete guaianolide scaffolds with 5/7/5 tricyclic system [11,12]. Recently, we have reported four unprecedented skeleton of 1,10-4,5-diseco-guaianolide involved hetero DSs with significant cytotoxic effect [13]. In our continuing efforts to search for novel bioactive polymeric terpenes, four novel hetero dimeric [4 + 2] adducts, artemisianins A-D (**1**–**4**), together with their putative biosynthetic precursors **5** and **6** were isolated from the leavers of *A. argyi*. This paper describes the details of the isolation and structure deduction of all isolates, as well as their cytotoxicity toward human cancer cell lines. Moreover, compound **1**-induced apoptotic mechanism is discussed.

## 2. Experimental section

### 2.1. General experimental procedures

Optical rotations were measured on a JASCO P-1020 polarimeter in MeOH at room temperature. ECD data were recorded on a Jasco spectrometer (Jasco, Tokyo, Japan). Nuclear magnetic resonance (NMR) spectra were on a Bruker AVIII-600 NMR instrument ($^1$H: 600 MHz, $^{13}$C: 150 MHz) (Bruker, Karlsruhe, Germany), with tetramethylsilane (TMS) as an internal standard. High-resolution electrospray ionizations (HRESIMS) were carried out an Agilent 6529B Q-TOF instrument (Agilent Technologies, Santa Clara, CA, USA). Preparative high-performance liquid chromatography (Pre-HPLC) was performed on a Shimadzu LC-6A system (Shimadzu, Tokyo, Japan) equipped with a Shim-pack RP-$C_{18}$ column (200 mm × 20 mm i.d., 10 μm, Shimadzu, Tokyo, Japan) with flow rate at 10.0 ml/min, detected by a binary

* Corresponding authors.
*E-mail addresses:* luojg@cpu.edu.cn (J.-G. Luo), cpu_lykong@126.com (L.-Y. Kong).

https://doi.org/10.1016/j.bioorg.2018.11.013
Received 16 October 2018; Received in revised form 12 November 2018; Accepted 12 November 2018
Available online 01 December 2018

channel UV detector at 210 and 230 nm. All solvents used were of analytical grade (Jiangsu Hanbang Science and Technology. Co., Ltd.). MCI (Mitsubishi, Japan) and RP-$C_{18}$ silica (40–63 μm, FuJi, Japan) were used for column chromatography.

### 2.2. Plant material

The leaves of *A. argyi* were collected from Qichun County, Hubei Province, People's Republic of China. The sample was identified by professor Mian Zhang (China Pharmaceutical University). A specimen (NO. 150520) was deposited in the Department of Natural Medicinal Chemistry, China Pharmaceutical University.

### 2.3. Extraction and isolation

The crude extract of *A. argyi* was treated as previously reported to produce Fr1-Fr6 [13]. Subsequently, Fr2 (5.1 g) was subjected to RP-$C_{18}$ CC (80 g, eluted with 20–100% MeOH, v/v) to produce Fr2.1-Fr2.5, and Fr2.2 was further purified by preparative HPLC using 48% MeOH/$H_2O$ (v/v) as mobile phase to yield compounds **1** (9.2 mg, $t_R$ = 27.8 min), and **2** (5.3 mg, $t_R$ = 25.9 min) and subfraction Fr2.2.1. The subfraction Fr2.2.1 was further purified by preparative HPLC eluted with 36% MeCN/$H_2O$ (v/v) to product compound **3** (7.8 mg, $t_R$ = 34.9 min) and **4** (6.5 mg, $t_R$ = 32.5 min). Fr2.4 (1.3 g) was subjected to a RP-$C_{18}$ CC to yield fractions Fr2.4.1-Fr2.4.6. The further isolation of Fr2.4.1 using 30% MeOH/$H_2O$ yielded **5** (18.1 mg, $t_R$ = 23.4 min) and **6** (25.3 mg, $t_R$ = 22.8 min).

#### 2.3.1. Artemisianin A (1)

colorless gum; $[\alpha]_D^{25}$-39.8 (*c* 0.1, MeOH); UV (MeOH) $\lambda_{max}$ (log $\varepsilon$) 209 (4.09) nm; ECD (MeOH) $\lambda_{max}$ ($\Delta\varepsilon$) 228 (−3.7), 348 (+0.4) nm; IR (KBr) $\nu_{max}$ 3439, 1760, 1712, 1633, 1383, 1265, 1160, 985, 731 $cm^{-1}$; $^1$H- and $^{13}$C NMR data, see Table S1; (+)-ESIMS *m/z* 525 $[M+H]^+$; HRESIMS $[M+Na]^+$ at *m/z* 547.2301 (calcd for $C_{30}H_{36}O_8Na$, 547.2302).

#### 2.3.2. Artemisianin B (2)

colorless gum; $[\alpha]_D^{25}$-53.8 (*c* 0.1, MeOH); UV (MeOH) $\lambda_{max}$ (log $\varepsilon$) 210 (4.14) nm; ECD (MeOH) $\lambda_{max}$ ($\Delta\varepsilon$) 226 (−3.5), 324 (+0.4) nm; IR (KBr) $\nu_{max}$ 3444, 1759, 1711, 1382, 1267, 1149, 983, 731 $cm^{-1}$; $^1$H- and $^{13}$C NMR data, see Table S1; (+)-ESIMS *m/z* 525 $[M+H]^+$; HRESIMS $[M+Na]^+$ at *m/z* 547.2309 (calcd for $C_{30}H_{36}O_8Na$, 547.2302).

#### 2.3.3. Artemisianin C (3)

colorless gum; $[\alpha]_D^{25}$-11.2 (*c* 0.1, MeOH); UV (MeOH) $\lambda_{max}$ (log $\varepsilon$) 209 (4.25) nm; ECD (MeOH) $\lambda_{max}$ ($\Delta\varepsilon$) 228 (−17.6), 336 (+2.0) nm; IR (KBr) $\nu_{max}$ 3453, 1755, 1708, 1647, 1458, 1383, 1264, 1162, 1128, 985 $cm^{-1}$; $^1$H- and $^{13}$C NMR data, see Table S1; (+)-ESIMS *m/z* 525 $[M+H]^+$; HRESIMS $[M+Na]^+$ at *m/z* 547.2298 (calcd for $C_{30}H_{36}O_8Na$, 547.2302).

#### 2.3.4. Artemisianin D (4)

colorless gum; $[\alpha]_D^{25}$-55.6 (*c* 0.1, MeOH); UV (MeOH) $\lambda_{max}$ (log $\varepsilon$) 210 (4.21) nm; ECD (MeOH) $\lambda_{max}$ ($\Delta\varepsilon$) 207 (−3.2), 230 (+1.1) nm; IR (KBr) $\nu_{max}$ 3460, 1753, 1702, 1643, 1457, 1385, 1266, 1164, 986 $cm^{-1}$; $^1$H- and $^{13}$C NMR data, see Table S1; (+)-ESIMS *m/z* 525 $[M+H]^+$; HRESIMS $[M+Na]^+$ at *m/z* 547.2304 (calcd for $C_{30}H_{36}O_8Na$, 547.2302).

### 2.4. Quantum chemical ECD calculation

Systematic conformational analyses for **1–4** were performed via Gaussian 09 program package [13]. The conformers were optimized using the TD-SCF method at the B3LYP/6-311 + G(d, 2p) basis set level. The stationary points have been checked as the true minima of the potential energy surface by verifying they do not exhibit vibrational imaginary frequencies. The stable conformers without imaginary frequencies were subjected to ECD calculation by the TDDFT method at the B3LYP/6-311 + G(d, 2p) level in MeOH as solvent. ECD spectra of different conformers were simulated using SpecDis with a half-bandwidth of 0.3 eV, and the final ECD spectra were obtained according to the Boltzmann-calculated contribution of each conformer. The systematic errors in the prediction of the wavelength and excited-state energies are compensated for by employing UV correction. The calculated ECD spectra were compared with the experimental data.

### 2.5. Cytotoxicity assay

Cytotoxicity of compounds **1–4** against the human colon (HT-29, HCT-116) and breast cancer (MCF-7) cell lines was evaluated using the MTT method [13]. Oxaliplatin was used as the positive control.

### 2.6. Measurement of intracellular $Ca^{2+}$ level

Calcium measurements were performed on attached populations of HT-29 cells. HT-29 cells pretreated with compound **1** (5.0, 10.0, 15.0 μM) for 24 h were treated with 20 mM glutamate for 30 min. The cells were washed twice with PBS and incubated with 5 μM fluo-4 AM in Krebs-Ringer buffer (D-glucose 10 mM, NaCl 120 mM, KCl 4.5 mM, $Na_2HPO_4$ 0.7 mM, $NaH_2PO_4$ 1.5 mM and $MgCl_2$ 0.5 mM, pH 7.4) for 30 min at 37 °C in the dark. The cells were then washed twice with PBS and incubated for additional 20 min at 37 °C. Finally, the cells images were analyzed by ImageXpress® Micro Confocal (Molecular Devices, Sunnyvale, CA).

### 2.7. Endoplasmic reticulum (ER)-tracker and Hoechst 33258 staining

Endoplasmic reticulum and Hoechst 33258 staining was performed according to the instructions of the manufacturer of ER-tracker kit and Hoechst 33258, respectively. Briefly, cells were washed with Hank's Balanced Salt Solution (HBSS, Gibco, Grand Island, NY, USA) or PBS and then incubated in pre-warmed ER-tracker (1 μM) or Hoechst 33258 (20 nM) dye solution for approximately 30 min at 37 °C. After HBSS or PBS washes, cells were then observed using a ImageXpress® Micro Confocal.

### 2.8. Western blot analysis

HT-29 cells were lysed in RIPA lysis buffer (50 mM Tris-HCl, pH 7.4, 150 mM NaCl, 0.25% deoxycholic acid, 1% NP-40, 1 mM EDTA, and protease inhibitors) (Amresco, Solon, OH), incubated on ice for 30 min, and centrifuged at 12,000 rpm at 4 °C for 15 min. The supernatant extracts were quantified for proteins by BCA assay (Beyotime Institute of Biotechnology, Jiangsu, China). Proteins were resolved on SDS-polyacrylamide gel and transferred to a polyvinyldenefluoride (PVDF) membrane (Bio-Rad Laboratories, Hercules, USA). Non-specific sites on the membrane were blocked with 5% skimmed milk in TBST buffer for 2 h at room temperature and then the membranes were incubated with protein-specific antibodies overnight at 4 °C. After washing twice with TBST buffer, the membranes were incubated in HRP conjugated secondary antibody solution for 2 h. Finally, immune complexes were visualized by ChemiDOC™ XRS + system (Bio-Rad Laboratories, Hercules, CA).

## 3. Results and discussion

Artemisianin A (1) was obtained as a colourless gum. A sodium adduct ion peak at *m/z* 547.2301 ($[M+Na]^+$, calcd for $C_{30}H_{36}O_8Na$, 547.2302) in the positive-ion HRESIMS suggested its molecular formula of $C_{30}H_{36}O_5$, corresponding with 13 indices of hydrogen deficiency. The IR spectrum showed absorption bands for hydroxy (3493 $cm^{-1}$), ester

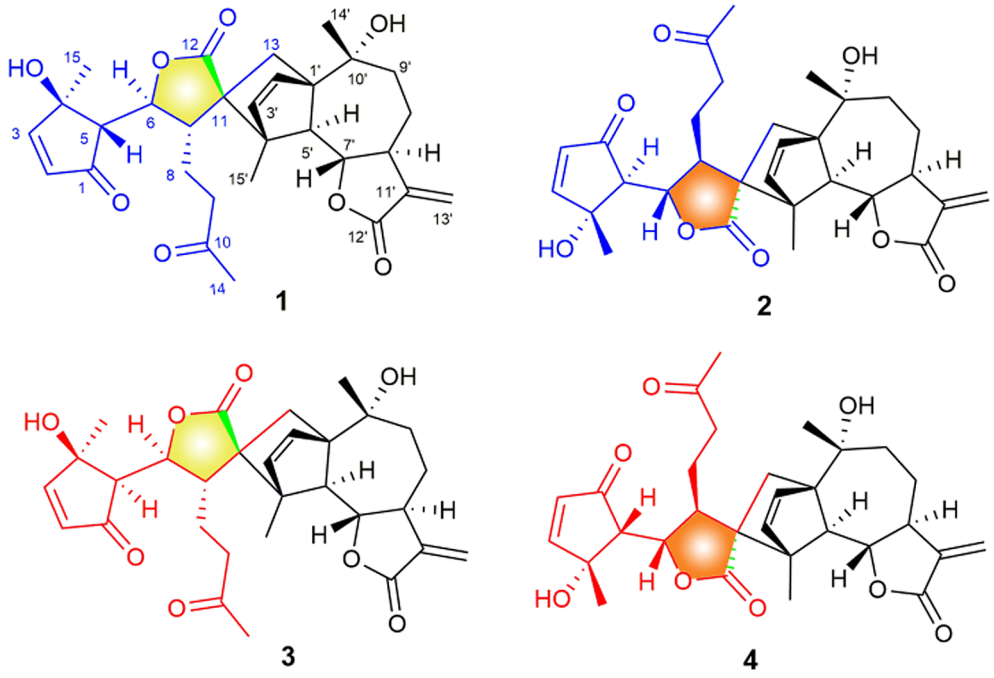


**Fig. 1.** Structures of compounds **1**–**4**.

carbonyl (1760 $cm^{-1}$), and carbonyl (1712 $cm^{-1}$) functionalities. The $^1H$ NMR spectrum displayed characteristic signals as follow: a pair of typical exocyclic methylene group ($\delta_H$ 5.39, d, $J$ = 3.2 Hz; 6.11, d, $J$ = 3.2 Hz), two *cis*-double bonds ($\delta_H$ 6.12, 7.48, each, d, $J$ = 5.8 Hz; 5.98, 6.02, each, d, $J$ = 5.8 Hz), two oxy-methines ($\delta_H$ 4.38, t, $J$ = 7.5 Hz; $\delta_H$ 4.14, t, $J$ = 10.0 Hz), and four methyls ($\delta_H$ 1.35, s; 1.42, s; 1.56, s; 2,17, s) (Table S1). The $^{13}C$ NMR with the assistance of HSQC spectroscopic data demonstrated the presence of 30 carbon resonances, comprising four methyls, six methylenes, ten methines, and ten quaternary carbons, in which included two ester carbonyls, two carbonyls, four oxygenated and six olefinic carbons (Table S1). The above-mentioned information, in combination with its HRESIMS data, implied that **1** must be a DS (Fig. 1) [13,14].

The structure of **1** was established on the basic analysis of HMBC data. The HMBC cross-peaks from H-2 and H-3 to C-1, C-4, and C-5, $H_3$-15 to C-3 and C-5, H-5 to C-1, C-2, C-3, and C-7, H-6 to C-8, C-11, and C-12, H-7 to C-9, C-12, and C-13, and $H_3$-14 to C-9 and C-10 (Fig. 2) suggested that the fraction of unit A was identical to that of seco-tanapartholide A (**5**) co-isolated from this plant [15]. The remaining unit B was constructed by the similar HMBC analysis. The HMBC correlations of H-5′/C-2′, C-3′, C-7′, and C-10′, H-6′/C-1′, C-4′, C-7′, and C-11′, $H_3$-14′/C-1′ and C-9′, $H_3$-15′/C-3′ and C-5′, and the exocyclic olefinic protons of $H_2$-13′/C-7′ and C-12′ were observed (Fig. 2), which indicated unit B of **1** was a guaia-2(3),11(13)-dien-12-olic lactone-like moiety [8,16]. In the HMBC spectrum, the correlations of geminal methylene $H_2$-13 ($\delta_H$ 1.50, 2.46, each, d, $J$ = 12.3 Hz) with C-1′ ($\delta_C$ 64.7), C-2′ ($\delta_C$ 135.4), and C-10′ ($\delta_C$ 73.2) (Fig. 2) suggested that C-13 ($\delta_C$ 38.2) was directly attached to C-1′, while correlations of H-5′ and H-15′ ($\delta_H$ 1.42, s) with the quaternary carbon C-11 ($\delta_C$ 60.3) indicated the linkage of C-11 and C-4′ ($\delta_C$ 56.7). Thus, the new formative bicyclic [2.2.1] hept-2-ene core is explicable by a [4 + 2] Diels-Alder cycloaddition between a guaianolide unit B and a 1,10-seco-guaianolide unit A.

The relative configuration of **1** was determined by the analysis of coupling constants and the correlations detected in its NOESY spectrum (Fig. 2). In the unit B, the large coupling constants of H-5′/H-6′, H-6′/H-7′ ($J_{5',6'} = J_{6',7'}$ = 10.0 Hz) revealed their *trans* relationships [9], and H-5′ and H-7′ were assigned as $\alpha$-orientation according to the NOE correlations of H-5′/H-7′, thus H-6′ was defined to be $\beta$-oriented. The NOE correlations of H-6′/H-9′$\beta$, H-9′$\beta$/H-2′, H-2′/$H_3$-14′ (Fig. 2) demonstrated the 2′$\beta$,3′$\beta$-ethylidene bridge in the formative five-membered ring C-1′–C-13–C-11–C-4′–C-5′ and 14′$\beta$-$CH_3$ in the cycloheptane. In the unit A, the NOE correlations from H-5′ to H-13$\alpha$, H-13$\alpha$ to H-8, H-8 to H-6, H-6 to $H_3$-15, and $H_3$-15′ to H-5 and H-7 (Fig. 2) suggested that H-6 and H-15 were $\alpha$-oriented, while H-5 and H-7 were $\beta$-oriented. The results were in good agreement with those NOE correlations in seco-tanapartholides A. Thus, at this point, the relative configuration of **1**

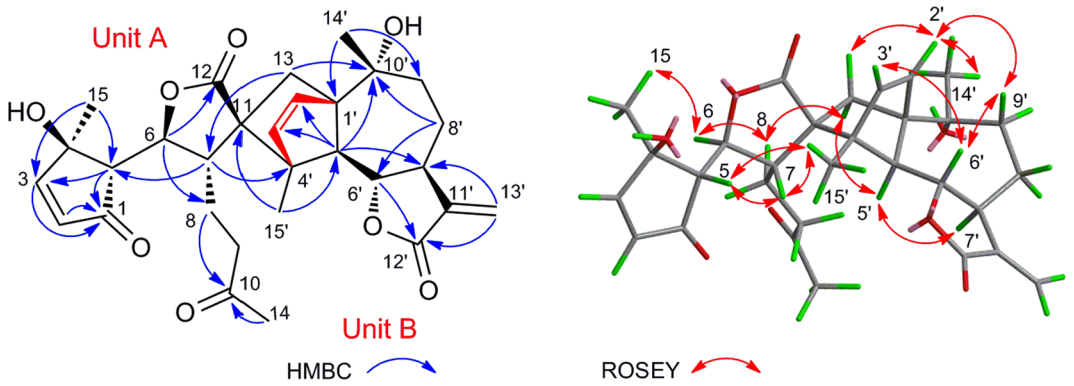


**Fig. 2.** Key HMBC and NOESY correlations of compound **1**.

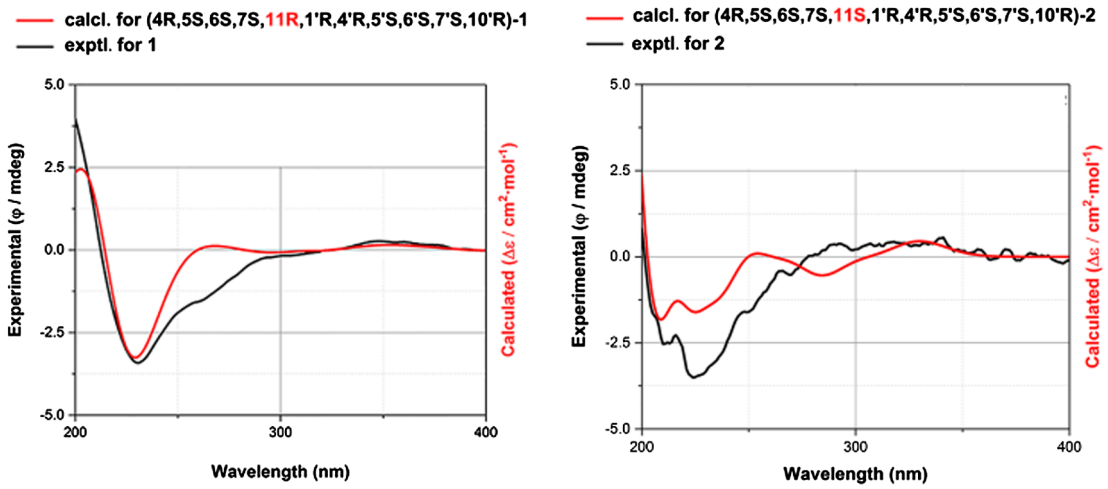


**Fig. 3.** Experimental ECD spectra for **1** and **2** in MeOH along with their possible absolute configuration of calculated ECD spectra based on internal energies with free energy corrections after optimization at the B3LYP/6-311 + G (d, 2p) level with the polarizable continuum model in MeOH.

was confirmed. The absolute configuration of **1** was determined by the quantum chemical calculation of the electronic circular dichroism (ECD) spectra using TDDFT at the B3LYP/6-311 + G(d, 2p) level in MeOH solution with the CPCM model [17]. As shown in Fig. 3, the calculated ECD spectrum of (4*R*,5*S*,6*S*,7*S*,11*R*,1′*R*,4′*R*,5′*S*,6′*S*,7′*S*,10′*R*)-**1** was agreed well with the experimental spectrum leading to the assignment of the absolute configuration at stereogenic centers. Thus, the structure of **1** was elucidated as shown, named artemisianin A.

The planar structure of **2**, artemisianin B, was identical to that of **1** dimerized from Diel-Alder cyclization by comparison of their HRESIMS (*m/z* 547.2309 $[M+Na]^+$, calcd for $C_{30}H_{36}O_8Na$, 547.2302) and NMR data. In the NOESY spectrum, the correlations of H-5/H-7, H-6/H-15 in unit A, as well as H-5′/H-7′, H-6′/H-9′*β*, H-9′*β*/H-2′, and H-2′/H-14′ in unit B, allowed the assignments of the relative configuration of units A and B in **2** to be consistent with those of in **1**. The NOE relations of H-7/H-13*β*, H-6/H-15′, and H-8*β*/H-3′ (Fig. 4) proved that these two units was linked in a different mode (Scheme 1), with main difference from **1** being of chiral center at C-11. The absolute configuration of **2** was also determined by ECD calculation method. According to the calculated ECD results (Fig. 3), the 4*R*,5*S*,6*S*,7*S*,11*S*,1′*R*,4′*R*,5′*S*,6′*S*,7′*S*,10′*R* configurations of **2** was defined as shown.

Artemisianin C (**3**), obtained as a colourless gum, had a molecular formula of $C_{30}H_{36}O_8$ based on the (+) HRESIMS ion at *m/z* 547.2298 ($[M+Na]^+$, calcd for 547.2302). Detailed analysis of the 1D and 2D NMR data of **3** suggested that the structure of **3** was comprised from the similar guaianolide units as those of **1**, while the obvious differences between **3** and **1** were in unit A. In their $^1H$ NMR spectra of unit A, the chemical shift and coupling constant at H-5 ($\delta_H$ 2.68, s) in **3** was observed, whereas H-5 in **1** was $\delta_H$ 3.03 (d, $J$ = 7.5 Hz). This suggested that **3** may be a C-5 epimer of **1**. In the NOESY spectrum of **3**, the correlations of H-5/H-6, H-5/H-8, H-5/H-15, and H-6/15 (Fig. 4) demonstrated the *α*-orientation of H-5, contracted to **1**, and thus structure of unit A is same as the co-occurrence of monomeric sesquiterpene **6** [15]. The experimental ECD curve of **1** was nearly identical to the calculated one in the Fig. S1, suggesting the 4*R*,5*R*,6*S*,7*S*,11*R*,1′*R*,4′*R*,5′*S*,6′*S*,7′*S*,10′*R* configurations for **3**.

The molecular formula of artemisianin D (**4**) was identical to those of **1**–**3**, as deduced from the quasi-molecular ion peak (*m/z* 547.2304 $[M+Na]^+$, calcd for $C_{30}H_{36}O_8Na$, 547.2302) in HRESIMS. The NMR data indicated that compound **4** was constituted by same units A and B as **3**. Differently, their Diels-Alder addition formation led to the contrary configuration at C-11 ($\delta_C$ 55.8). This was further consolidated by the NOE correlations of H-15′ ($\delta_H$ 1.51, s)/H-6 ($\delta_H$ 4.61, d, $J$ = 10.5 Hz), H-3′ ($\delta_H$ 6.03, d, $J$ = 5.8 Hz)/H-8*β* ($\delta_H$ 2.01, m) (Fig. S4-8). The experimental ECD spectrum of **4** resembled the calculated ECD curve (Fig. S1), suggesting the 4*R*,5*R*,6*S*,7*S*,11*S*,1′*R*,4′*R*,5′*S*,6′*S*,7′*S*,10′*R* configurations. Thus, the structure of **4** was established as in Fig. 1.

In summary, these four DSs could be divided into two groups for **1**, **3** and **2**, **4**, which were formed from the different [4 + 2] Diels-Alder cycloaddition model. For **1** and **3**, as showed in Scheme 1, the *α*-orientation of *α*-methylene-γ-lactone for dienophiles (**5** and **6**) would react with the 1′,4′-dienes of unit B from the α-side to yield **1** and **3** with 11*R* configuration. For **2** and **4**, while the *β*-orientation of dienophiles (unit A) attacked the dienes (unit B) also from the *α*-side to produce compounds **2** and **4** with 11*S* configuration. Because of the steric repulsions caused by methyl group at $CH_3$-14′, dienophiles for **5** and **6** would be prone to attack dienes of unit B from the reverse side of the methyl group, resulting in *R* and *S* configuration at C-11, respectively [5].

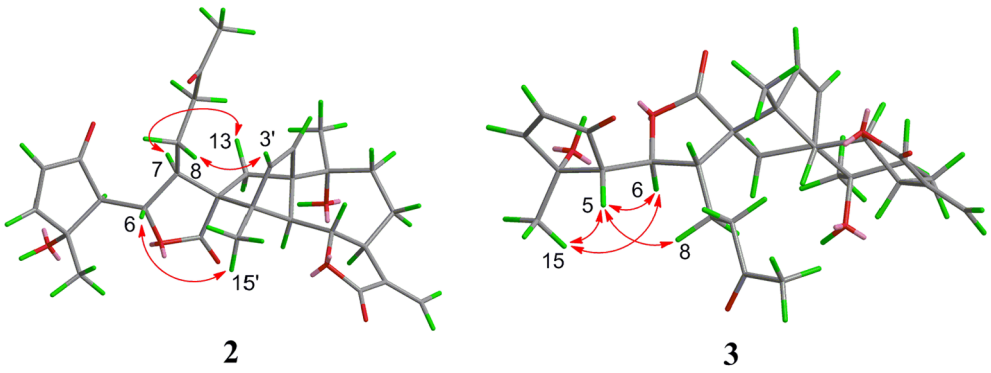


**Fig. 4.** Key ROESY correlations of compounds **2** and **3**.

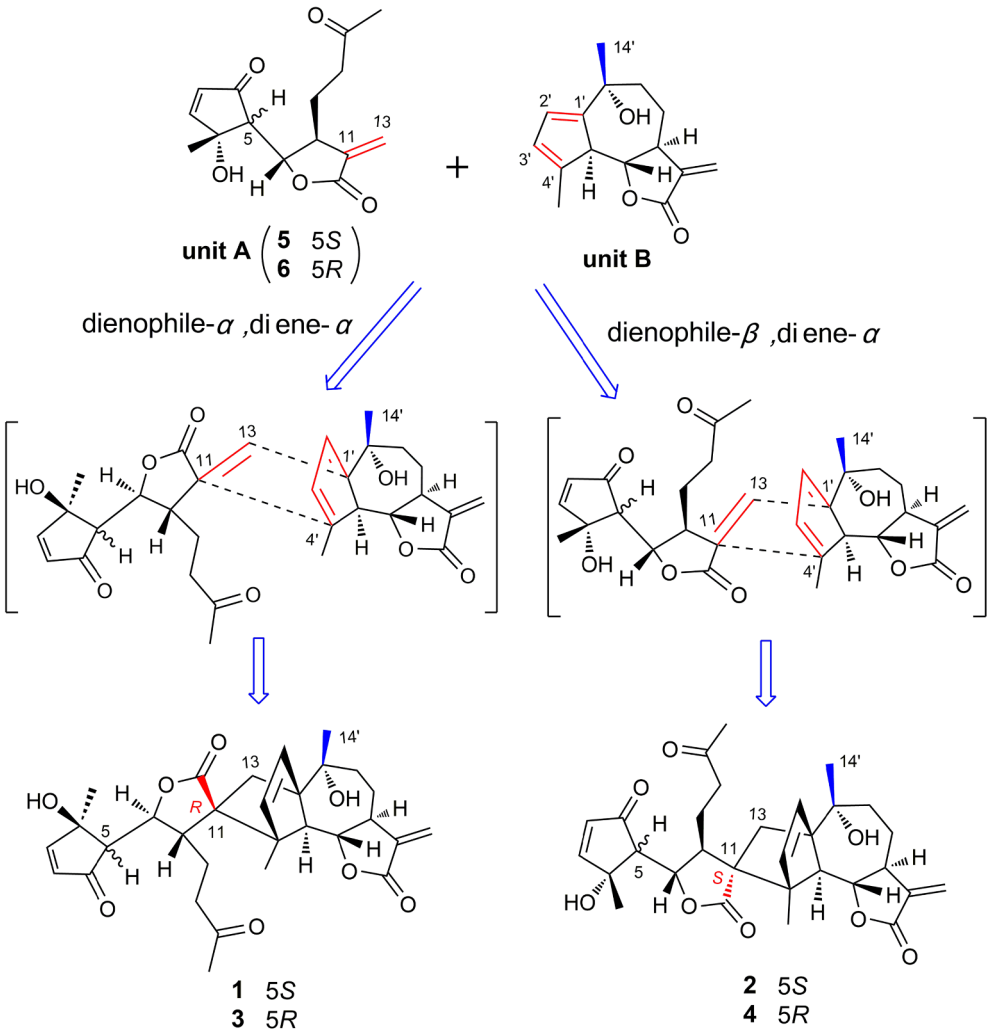


**Scheme 1.** Plausible biosynthetic pathways of **1**–**4**.

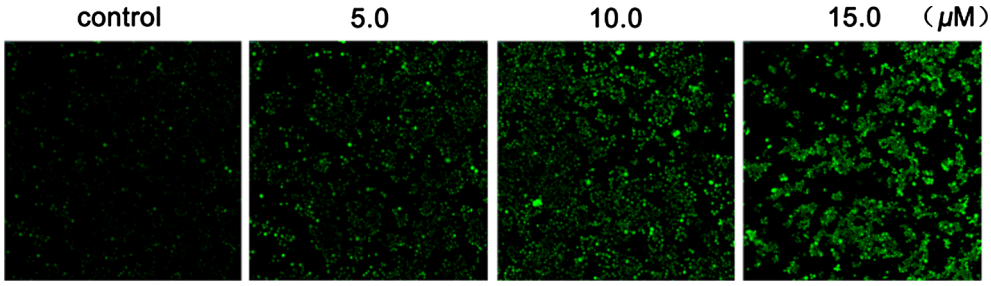


**Fig. 5.** Effects of compound **1** (5.0, 10.0, 15.0 μM) on intracellular $Ca^{2+}$ fluorescence intensities incubated with 5.0 μM fluo-4 AM in HT-29 cells. Control group was treated with DMSO only, the treated with fluo-4 AM.

As the cytotoxic activity of DSs are widely investigated [4,5], compounds **1**–**4** were tested their cytotoxicities in human colon (HT-29, HCT-116) and breast cancer (MCF-7) cell lines by MTT assay. The screening results are expressed as $IC_{50}$ values. As shown in Table S2, compound **1** displayed potent inhibitory effect against HT-29 cell line with an $IC_{50}$ value of 7.2 μM. Furthermore, HT-29 cells were treated with **1** at concentration of 5.0, 10.0 and 15.0 μM, and apoptotic nuclear chromatin condensation was examined with Hoechst 33342 staining. Compared with the control group, chromatin condensation was distinctly detected in treatment of **1** at 10.0 and 15.0 μM (Fig. S2). These results suggested that **1**-induced cytotoxicity was mediated by cell apoptosis.

Intracellular $Ca^{2+}$ is a key regulator of many cellular processes [18]. To evaluate the mechanism of **1**-induced apoptosis in HT-29 cells, efforts were made to explore whether compound **1** could affect cellular $Ca^{2+}$ homeostasis in HT-29 cells. Notably, the $Ca^{2+}$ fluorescence intensity increased when the cells were treated with **1** (Fig. 5). As is well known, the imbalance $Ca^{2+}$ in cellular homeostasis is one of an important factor to cause endoplasmic reticulum stress (ERs) [19]. Therefore, to illustrate the triggered ERs by **1** induced the apoptosis of HT-29 cells, we first characterized the morphological change of ER using ER-tracker staining, and the enlarged ER was observed (Fig. 6). In addition, in the Western blotting assay, as shown in Fig. 7, compound **1** upregulated ERs markers of glucose-regulated protein GRP78. These

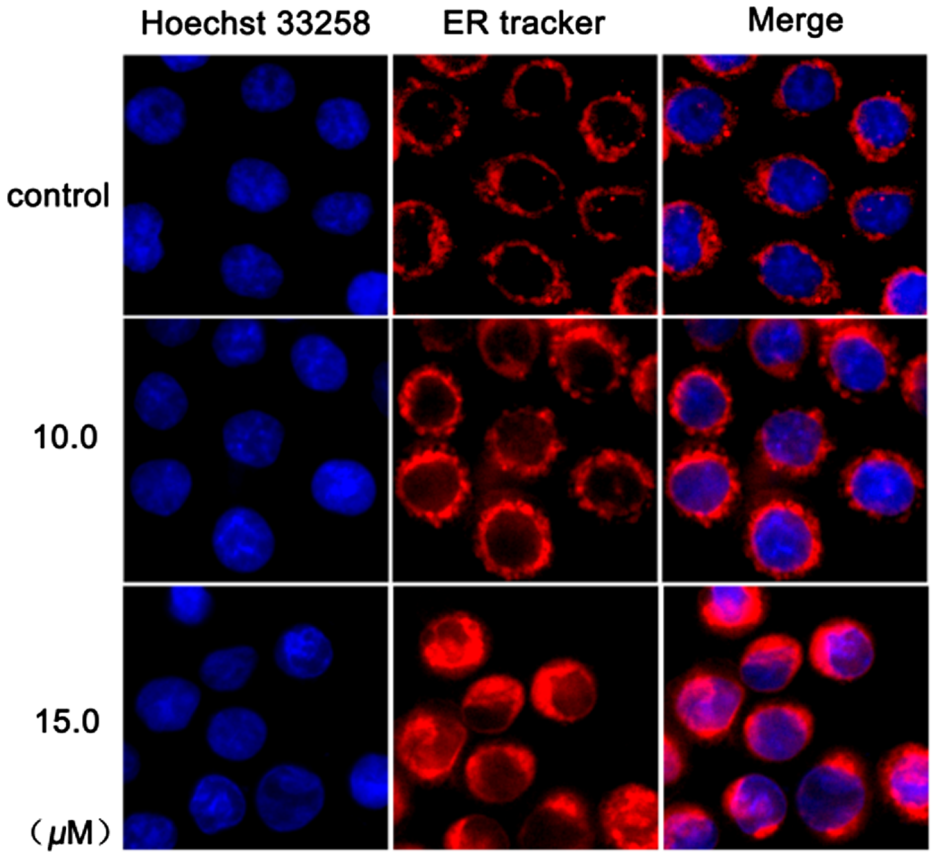


**Fig. 6.** Cells incubated with vehicle (control) or compound **1** (10.0, 15.0 μM) for 24 h, then stained with ER-tracker and Hoechst 33258, and observed by ImageXpress® Micro Confocal.

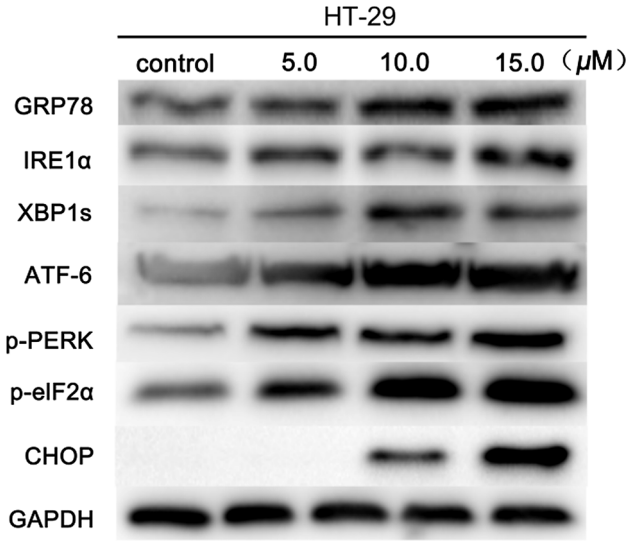


**Fig. 7.** The involvement of ER-stress signaling pathway in **1** induced apoptosis in HT-29 cells. Cells were treated with **1** (5.0, 10.0, 15.0 μM) for indicated time points prior to preparation of lysates, followed by Western blotting to detect the protein levels of GRP78, CHOP, IRE1α, XBP1s, p-PERK, p-eIF2α, and ATF6. GAPDH was used as an equal loading control.

results suggested that ERs was involved in the regulation of the cancer cell apoptosis [20].

The unfolded protein response (UPR) is a well-known characteristic of ER pathway [21]. Thus, the response of ERs was further assayed by the Western blotting of representative proteins for UPR. As shown in Fig. 7, it was clear to note that the expression of inositol requiring enzyme 1*α* (IRE1*α*) and X-box binding protein (XBP1s) were increased, indicating the activation of the IRE1*α* branch of UPR signaling. Moreover, the upregulation of auto-phosphorylated PKR-like endoplasmic reticulum resident kinase (p-PERK) and PERK-mediated phosphorylation of eukaryotic initiation factor (p-eIF2α) suggested that **1** engaged the PERK branch of UPR signaling, and the high expression in ATF6 level indicated that the ATF6 branch of UPR signaling was also involved (Fig. 7). The C/EBP homologous protein (CHOP), called the growth arrest and DNA damage induced gene-153 (GADD153), is one of the most important regulatory protein of the ERs induced apoptotic cell death [22]. As shown in Fig. 7, the level of CHOP expression is also elevated. Altogether, these results indicate that **1** inducted apoptosis in HT-29 via disruption of $Ca^{2+}$ homeostasis to activate the ER-stress apoptosis signaling.

## 4. Conclusions

In this report, artemisianins A-D (**1**–**4**), hetero sesquiterpenoid dimers with a 1,10-seco-guaianolide unit, together with their possible precursors **5**–**6**, were isolated from the famous traditional Chinese medicine *A. argyi*. To our best knowledge, the representative natural product of **1** was the first DS reported to exhibit antitumor activity via the activated ER stress pathway. These results would provide a clue for exploiting DSs as a promising agent for the treatment of colon cancer in a new way.

## Conflict of interest

The authors declare no conflicts of interest.

## Acknowledgements

This research work was financially supported by the Program for Changjiang Scholars and Innovative Research Team in University (IRT_15R63), the Priority Academic Program Development of Jiangsu Higher Education Institutions (PAPD), and the 111 Project from Ministry of Education of China and the State Administration of Foreign Export Affairs of China (No: B18056).

## Appendix A. Supplementary material

Supplementary data to this article can be found online at https://doi.org/10.1016/j.bioorg.2018.11.013.

## References

[1] Z.J. Zhan, Y.M. Ying, L.F. Ma, W.G. Shan, Org. Chem. Front. 4 (2017) 2102–2108.
[2] Y.X. Yang, S. Gao, S.D. Zhang, X.P. Zu, Y.H. Shen, L. Shan, H.L. Li, W.D. Zhang, RSC Adv. 5 (2015) 55285–55289.
[3] X.D. Zhou, X.Y. Chai, K.W. Zeng, M.B. Zhao, Y. Jiang, P.F. Tu, Tetrahedron Lett. 56 (2015) 1141–1143.
[4] Y.X. Yang, L. Shan, Q.X. Liu, Y.H. Shen, J.P. Zhang, J. Ye, X.K. Xu, H.L. Li, W.D. Zhang, Org. Lett. 16 (2014) 4216–4219.
[5] J.W. Wu, C.Q. Tang, L. Chen, Y. Qiao, M.Y. Geng, Y. Ye, Org. Lett. 17 (2015) 1656–1659.
[6] C. Zhang, S. Wang, K.W. Zeng, J. Li, D. Ferreira, J.K. Zjawiony, B.Y. Liu, X.Y. Guo, H.W. Jin, Y. Jiang, P.F. Tu, J. Nat. Prod. 79 (2016) 213–223.
[7] Z.J. Wu, X.K. Xu, Y.H. Shen, J. Su, J.M. Tian, S. Liang, H.L. Li, R.H. Liu, W.D. Zhang, Org. Lett. 10 (2008) 2397–4000.
[8] K. Zan, X.Y. Chai, X.Q. Chen, Q. Wu, Q. Fu, S.X. Zhou, P.F. Tu, Tetrahedron 68 (2012) 5060–5065.
[9] J. Wen, H.M. Shi, Z.R. Xu, H.T. Chang, C.Q. Jia, K. Zan, Y. Jiang, P.F. Tu, J. Nat. Prod. 73 (2010) 67–70.
[10] A. Turak, S.P. Shi, Y. Jiang, P.F. Tu, Phytochemistry 105 (2014) 109–114.
[11] S.H. Lee, H.K. Kim, J.M. Seo, H.M. Kang, J.H. Kim, K.H. Son, H. Lee, B.M. Kwon, J. Shin, Y. Seo, J. Org. Chem. 67 (2002) 7670–7675.
[12] S.H. Lee, M.Y. Lee, H.M. Kang, D.C. Han, K.H. Son, D.C. Yang, N.D. Sung, C.W. Lee, H.M. Kim, B.M. Kwon, Bioorgan. Med. Chem. 11 (2003) 4545–4549.
[13] G.M. Xue, C. Han, C. Chen, L.N. Li, X.B. Wang, M.H. Yang, Y.C. Gu, J.G. Luo, L.Y. Kong, Org. Lett. 19 (2017) 5410–5413.
[14] Y. Li, M.C. Zhu, M.L. Zhang, Y.F. Wang, M. Dong, Q.W. Shi, C.H. Huo, F. Sauriol, H. Kiyota, Y.C. Gu, B. Cong, Tetrahedron Lett. 53 (2012) 2601–2603.
[15] K. Kawazoe, Y. Tsubouchi, N. Abdullah, Y. Takaishi, H. Shibata, T. Higuti, H. Hori, M. Ogawa, J. Nat. Prod. 66 (2003) 538–539.
[16] Q. Gu, Y.Y. Chen, H. Cui, D. Huang, J.W. Zhou, T.Z. Wu, Y.P. Chen, L.N. Shi, J. Xu, RSC Adv. 3 (2013) 10168–10172.
[17] L. Liu, Y. Han, J.H. Xiao, L. Li, L.D. Guo, X.J. Jiang, L.Y. Kong, Y.S. Che, J. Nat. Prod. 79 (2016) 2616–2623.
[18] B.Y. Fan, Y.C. Gu, Y. He, Z.R. Li, J.G. Luo, L.Y. Kong, J. Nat. Prod. 77 (2014) 2264–2272.
[19] X. Xiao, W.P. Qi, J.M. Clark, Y. Park, Food. Chem. Toxicol. 109 (2017) 123–129.
[20] C. Zhang, Y.N. Jiang, J. Zhang, J. Huang, J.H. Wang, Int. J. Mol. Sci. 16 (2015) 14979–14996.
[21] H. Urra, E. Dufey, T. Avril, E. Chevet, C. Hetz, Trends Cancer 2 (2016) 252–262.
[22] S.E. Chow, C.H. Kao, Y.T.A. Liu, M.L. Cheng, Y.W. Yang, Y.K. Huang, C.C. Hsu, J.S. Wang, Apoptosis 19 (2014) 527–541.